

ACCELERATING HIGH-ENERGY PULSAR RADIATION CODES

C. VENTER AND O. C. DE JAGER¹

Centre for Space Research, North-West University, Potchefstroom Campus, Private Bag X6001, Potchefstroom 2520, South Africa
 Received 2010 June 26; accepted 2010 October 21; published 2010 December 2

ABSTRACT

Curvature radiation (CR) is believed to be a dominant mechanism for creating gamma-ray emission from pulsars and is emitted by relativistic particles that are constrained to move along curved magnetic field lines. Additionally, synchrotron radiation (SR) is expected to be radiated by both relativistic primaries (involving cyclotron resonant absorption of radio photons and re-emission of SR photons), or secondary electron–positron pairs (created by magnetic or photon–photon pair production processes involving CR gamma rays in the pulsar magnetosphere). When calculating these high-energy spectra, especially in the context of pulsar population studies where several millions of CR and SR spectra have to be generated, it is profitable to consider approximations that would save computational time without sacrificing too much accuracy. This paper focuses on one such approximation technique, and we show that one may gain significantly in computational speed while preserving the accuracy of the spectral results.

Key words: pulsars: general – radiation mechanisms: non-thermal

1. INTRODUCTION

Curvature radiation (CR) arises when relativistic particles are constrained to move along curved orbits, for example, along magnetic field lines above a pulsar’s stellar surface (e.g., Harding 1981). This mechanism has played a central role in explaining high-energy (HE) emission in all the standard pulsar models: the polar cap (PC) model (Daugherty & Harding 1982, 1996) where radiation occurs very close to the neutron star surface, the outer gap (OG) model (Cheng et al. 1986; Romani 1996) with radiation originating above the null charge surface, in a gap which develops close to the last open field lines, and the slot gap (SG) model (Arons 1983; Muslimov & Harding 2003) with radiation coming from narrow gaps close to the last open field lines, extending from the stellar surface almost up to the light cylinder. Additionally, synchrotron radiation (SR) may also be emitted by secondary electron–positron pairs created in the magnetosphere via magnetic pair production in the SG (Harding et al. 2008) or via photon–photon pair production in the OG (e.g., Hirotani 2005). Predictions of inverse Compton scattering (ICS) components are more uncertain, but are typically of much lower flux compared to the SR and CR components (Bulik et al. 2000). Lastly, cyclotron resonant absorption of radio photons by relativistic primaries, followed by spontaneous SR, has been invoked for millisecond pulsar (MSP) modeling (Harding et al. 2005) as well as for the Crab (Harding et al. 2008).

The single-particle CR spectrum is characterized by a power law with a simple exponential cutoff (similar to the SR spectrum). A phase-averaged HE pulsar spectrum, which may be thought of as an averaged, cumulative spectrum involving the addition of many single-particle CR spectra which originate in different parts of the magnetosphere, is therefore expected to share common features with a single-particle spectrum. The *Fermi* Large Area Telescope (*Fermi*-LAT) has recently published its First Pulsar Catalog (Abdo et al. 2010a) containing nearly 50 gamma-ray pulsar detections and indeed fit their spectra using power laws with exponential cutoffs. The spectral cutoffs are around a few GeV, as expected for the case

of radiation-reaction-limited acceleration of relativistic electrons, where the acceleration rate equals the loss rate (e.g., Harding et al. 2005):

$$e|E_{||}| \sim \frac{2e^2\gamma_{\text{RR}}^4}{3\rho_c^2}. \quad (1)$$

Substituting $\gamma_{\text{RR}} = (1.5E_{||}/e)^{1/4}\rho_c^{1/2}$ into the expression for the cutoff energy (see Equation (9)), one obtains

$$E_{\gamma, \text{cutoff}} \sim 4 E_{||,4}^{3/4} \rho_{c,8}^{1/2} \text{ GeV}, \quad (2)$$

with $E_{||,4} = E_{||}/10^4$ statvolt cm^{-1} the electric field parallel to the magnetic field and $\rho_{c,8} = \rho_c/10^8$ cm the curvature radius. However, the power-law indices are typically much softer than the predicted index of $-2/3$ for monoenergetic, single-particle emission. This effect is believed to be due to superposition of many single-particle CR spectra from different field lines that add to give the observed spectrum. Also, when fitting a super-exponential spectral shape to the data (Nel & De Jager 1995),

$$\frac{dN}{dE} = K E^{-\Gamma} \exp \left[\left(-\frac{E}{E_c} \right)^b \right], \quad (3)$$

sometimes a value of $b < 1$ is obtained, as in the case of Vela, where $b = 0.68$ was found (Abdo et al. 2010b). This has been ascribed to the fact that E_c varies with phase, leading to an average spectrum that decreases slower with energy than exponentially.

Beyond making rough estimates of spectral shapes (indices and cutoffs) to demonstrate the plausibility of the CR mechanism in the context of HE pulsar models as described above, several million CR spectra may have to be generated in order to produce detailed, quantitative spectral predictions which may be compared with high-quality measurements of phase-averaged and phase-resolved gamma-ray spectra (e.g., Abdo et al. 2010a). Such computationally expensive calculations are needed, for example, if one intends to study radiation properties of a sizable population of pulsars (e.g., Story et al. 2007), or for examining the cumulative emission generated by an ensemble of MSPs believed to be responsible for the HE emission recently detected by *Fermi*-LAT from several globular clusters (GCs; Abdo et al.

¹ National Research Foundation Research Chair: Astrophysics and Space Science.

2009, 2010c). In addition to CR calculations, this also holds for computing X-ray to gamma-ray SR spectral components. It is therefore profitable to consider approximations that would save computational time without sacrificing too much accuracy.

The aim of this paper is twofold: first, we discuss an approximation technique for calculating CR and SR spectra efficiently and accurately. Second, this paper also serves to provide more details regarding previous calculations of pulsed CR gamma-ray fluxes expected from a population of MSPs in the GCs 47 Tucanae and Terzan 5 (Venter et al. 2009a). While we previously approximated the pulsed CR flux using delta functions (see Section 4.1) for the single-particle spectra (Venter & de Jager 2008), Venter et al. (2009a) used the approximation scheme presented below (Section 4.2) and deferred the details to this follow-up paper. The technique described below has wide applicability. It may be applied to any pulsar model where the B -field and E -field are specified, assuming that emission from the different radiation mechanisms may be calculated independently. In particular, we envision that this technique may be useful for three-dimensional particle acceleration models where $E_{||}$ is calculated at each position in the magnetosphere where acceleration takes place. (Note that this technique will not make any contribution in terms of reducing computation time in the context of purely geometrical models, which are commonly used to study pulsar light curves by postulating some emissivity at certain magnetospheric locations without making any quantitative assumptions about $E_{||}(r, \theta, \phi)$; see, e.g., Dyks & Rudak 2003; Venter et al. 2009b.) Beyond pulsar models, the technique may also be useful for cases where CR and/or SR are invoked to explain measurements of other astrophysical sources such as pulsar wind nebulae. Generally, the technique may improve calculation speed for any application where particle tracing is needed in order to calculate their acceleration, transport and subsequent radiation, and where enough information is available to model the ambient fields which determine these processes.

The paper is organized as follows: in Section 2, we summarize the standard CR expressions; we discuss the calibration of our code as well as our approximation technique in Section 3 and 4, respectively, while we present our results in Section 5. We discuss the meaning of the CR cutoff energy from theoretical and observational perspectives in Section 6. The spectral approximation technique has wider applicability, and we argue that it may also be extended to include synchrotron radiation (SR) in Section 7. Our conclusions follow in Section 8.

2. STANDARD CR EXPRESSIONS

There have been somewhat different approaches in the literature regarding the calculation of the CR spectrum. Jackson (1962) considers a particle moving instantaneously at a constant speed on a circular path. This approximation is valid when discussing radiation from extremely relativistic particles undergoing arbitrary accelerations. For the case of longitudinal acceleration along a B -field line with curvature radius ρ_c , the critical frequency is defined by Jackson (1962) as

$$\omega_{\text{CR}}^{\text{J}} \equiv \frac{3\gamma^3 c}{\rho_c}, \tag{4}$$

with γ the electron's Lorentz factor, and c the speed of light in vacuum. The power radiated per energy interval by a single

particle is then given by

$$\left(\frac{dP}{dE}\right)_{\text{CR}}^{\text{J}} = \frac{\sqrt{3}\alpha_f \gamma c}{2\pi\rho_c} \kappa^{\text{J}} \left(\frac{E_\gamma}{E_{\text{CR}}^{\text{J}}}\right) = \frac{P(\omega)}{\hbar}, \tag{5}$$

$$\kappa^{\text{J}}(x) \equiv 2x \int_{2x}^{\infty} K_{5/3}(x') dx', \tag{6}$$

$$E_{\text{CR}}^{\text{J}} = \hbar\omega_{\text{CR}}^{\text{J}} = \frac{3\hbar c \gamma^3}{\rho_c}, \tag{7}$$

with $P(\omega)$ the power spectrum per frequency ω , α_f the fine-structure constant, and $K_{5/3}$ the modified Bessel function of order $5/3$.

Other authors have used different definitions of $\kappa(x)$ and ω_{CR} (e.g., Harding 1981; Daugherty & Harding 1982; Cheng & Zhang 1996; Story et al. 2007; Venter et al. 2009b):

$$\omega_{\text{CR}} \equiv \frac{3\gamma^3 c}{2\rho_c} = \frac{\omega_{\text{CR}}^{\text{J}}}{2}, \tag{8}$$

$$E_{\text{CR}} = \hbar\omega_{\text{CR}} = \frac{3\hbar c \gamma^3}{2\rho_c} = \frac{3\lambda_c \gamma^3}{2\rho_c} m_e c^2, \tag{9}$$

with $\lambda_c = \hbar/(m_e c)$ the Compton wavelength. In this case, the instantaneous power spectrum (in units of $\text{erg s}^{-1} \text{erg}^{-1}$) is given by

$$\left(\frac{dP}{dE}\right)_{\text{CR}} = \frac{\sqrt{3}\alpha_f \gamma c}{2\pi\rho_c} \kappa \left(\frac{E_\gamma}{E_{\text{CR}}}\right), \tag{10}$$

and (Erber 1966)

$$\kappa(x) \equiv x \int_x^{\infty} K_{5/3}(x') dx' \tag{11}$$

$$\approx \begin{cases} 2.149 x^{1/3} & x \ll 1 \\ 1.253 x^{1/2} e^{-x} & x \gg 1. \end{cases} \tag{12}$$

Upon integrating Equation (10) over energy, one finds the total power radiated by the electron primary, which is also equal to the total CR loss rate of the electrons (see Equation (1)):

$$\int \left(\frac{dP}{dE}\right)_{\text{CR}} dE = \dot{E}_{\text{CR}} = -\frac{2e^2 c \gamma^4}{3\rho_c^2}. \tag{13}$$

The low-energy (LE) part of the CR photon spectrum may be written, using Equation (12), as (Story et al. 2007)

$$\left(\frac{dN}{dE}\right)_{\text{low}} = \frac{1}{dA E} \left(\frac{dP}{dE}\right)_{\text{CR}} \approx \frac{0.518\alpha_f}{dA \hbar^{1/3}} \left(\frac{c}{\rho_c}\right)^{2/3} E_\gamma^{-2/3}, \tag{14}$$

which is the same as Equation (7) of Harding et al. (2005) within a factor of ≈ 2 (apart from the factor $dA = \Delta\Omega d^2$, with $\Delta\Omega$ the beaming solid angle). Similarly, the HE CR photon spectrum becomes

$$\left(\frac{dN}{dE}\right)_{\text{high}} \approx \frac{0.282\alpha_f}{dA} \left(\frac{c}{\gamma\rho_c\hbar}\right)^{1/2} E_\gamma^{-1/2} e^{-E_\gamma/E_{\text{CR}}}. \tag{15}$$

The problem arises when the definitions of various quantities above are mixed. For example, Daugherty & Harding (1982);

Meszaros (1992) define the CR power spectrum as follows:

$$\left(\frac{dP}{dE}\right)_{\text{CR}} = \frac{1}{\hbar} \left(\frac{dI}{d\omega}\right) \left(\frac{c}{2\pi\rho_c}\right) = \frac{\sqrt{3}\alpha_f\gamma c}{2\pi\rho_c} \kappa^J \left(2\frac{\omega}{\omega_{\text{CR}}}\right), \quad (16)$$

and assume that $\kappa^J(x)$ is equal to the approximate forms of Equation (12), which is not the case. Furthermore, the extra factor of 2 in the argument of $\kappa^J(x)$ leads to an error of factor 4 in the normalization constant as well as the lower limit of the integral when calculating $(dP/dE)_{\text{CR}}$. Removing the extra factor of 2 in the argument of $\kappa^J(x)$, and using ω_{CR}^J instead of ω_{CR} , would solve the problem.

Another example occurs when Harding et al. (2008) state that they are using $E_{\text{CR}}/m_e c^2$, but in fact are using ω_{CR} . The latter seems to be a typo, but they also use $\kappa^J(x)$ instead of $\kappa(x)$, leading to a factor of 2 difference in normalization. However, their code correctly calculates the total number of CR photons emitted per unit time in an energy interval $dE = E_2 - E_1$ around an energy \bar{E}_{bin} (Venter et al. 2009b),

$$dn_{\gamma,\text{CR}} = \dot{N} dt \frac{\dot{E}_{\text{CR}}}{E_{\text{bin}}} \times \frac{\int_{E_1}^{E_2} \kappa(x) dx}{\int_{E_0}^{\infty} \kappa(x) dx}, \quad (17)$$

(with $E_0 \ll E_{\text{CR}}$, \dot{N} the injection rate of primaries from the stellar surface, and \bar{E}_{bin} measured in cgs units) so there is no impact on their CR spectra.

In summary, the following equalities hold:

$$\kappa^J \left(\frac{E_\gamma}{E_{\text{CR}}^J}\right) = \kappa \left(\frac{E_\gamma}{E_{\text{CR}}}\right) = \kappa^J \left(\frac{1}{2} \frac{E_\gamma}{E_{\text{CR}}}\right) = \kappa \left(2 \frac{E_\gamma}{E_{\text{CR}}^J}\right). \quad (18)$$

Much confusion can be ruled out by being consistent in the use of the various definitions of CR expressions.

3. CALIBRATION OF CODE

In order to verify the CR spectral calculation from our code, we calculated the CR power spectrum (see Equation (10)) using different techniques. Figure 1 shows the various spectra. The thick, gray line indicates our ‘‘calibration curve,’’ which was calculated using logarithmic integration (Venter 2008, see also the Appendix), and for $N = 10,000$ steps. This spectrum coincides with the low- x and high- x approximations of Equation (12) as indicated by thick dashed lines (with $x \equiv E_\gamma/E_{\text{CR}}$). The thin lines indicate spectra calculated using Simpson integration for linearly spaced x -values, for $N = 100, 500, 1000,$ and $10,000$ respectively. A larger number of steps N leads to better approximation of the calibration spectrum, as expected. Lastly, the dot-dashed line indicates a calculation using a combination of the approximate forms of $\kappa(x)$, as well as an interpolation of numeric tables for $\kappa(x)$, valid for intermediate values of x .

We draw two conclusions from this exercise. First, it is prudent to use a method (such as logarithmic integration, which uses logarithmically spaced x -values) which takes into account that spectra are usually displayed on graphs with logarithmic axes. This is evidenced by the fact that the logarithmic integration method gives very nearly the same spectrum as the calibration spectrum for only $N \sim 100$ steps, while the spectra calculated using Simpson integration do not approximate the calibration spectrum very well at low energies, even for $N \sim 10,000$. Second, our interpolated spectrum is quite satisfactory (we get an MISE value of 0.0041 when comparing the interpolated and

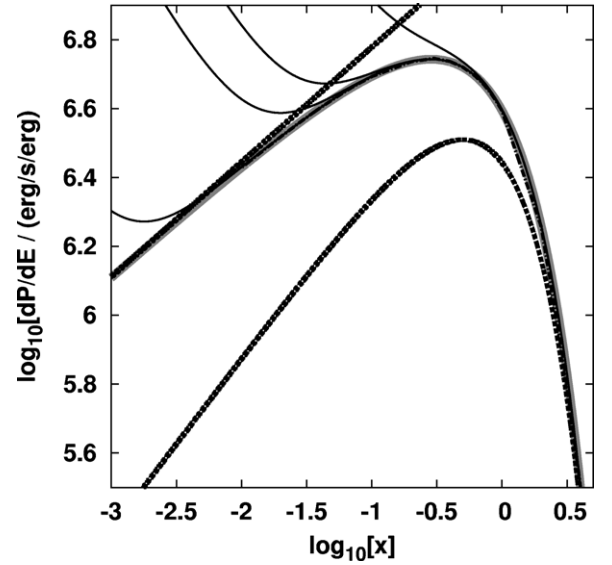


Figure 1. CR spectrum calculated using different techniques. The thick, gray line indicates our ‘‘calibration curve,’’ which was calculated using logarithmic integration and $N = 10,000$ steps. The thick dashed lines indicate the low- x and high- x approximations (with $x \equiv E_\gamma/E_{\text{CR}}$), while the thin lines indicate Simpson-integrated spectra for $N = 100, 500, 1000,$ and $10,000$ steps, respectively (spectra corresponding to larger N approximate the calibration spectrum better, as expected). Lastly, the dot-dashed line (barely visible at $x \sim 1$) indicates a calculation using a combination of the approximate forms of $\kappa(x)$, as well as an interpolation of numeric tables for $\kappa(x)$ valid for intermediate values of x .

calibration spectra; see Equation (27)), and does not need any numerical integration calculation. Therefore, we will be using this last method in what follows when calculating $\kappa(x)$ and the corresponding CR spectrum.

4. APPROXIMATION TECHNIQUE

4.1. Delta-function Approximation

To save computational time when computing CR gamma-ray spectra, we used the following approximation (e.g., Venter & de Jager 2008). First, we calculated the incremental photon luminosity dL_γ radiated in an incremental time dt by primary electrons, which are accelerated along a B -field line by the parallel E -field. We used the total radiated CR power per electron primary, \dot{E}_{CR} (Equation (13)):

$$dL_\gamma = \dot{N} dt \dot{E}_{\text{CR}}, \quad (19)$$

with $\dot{N} \approx c|\rho_{\text{GJ}}|dS/e$ the number of electron primaries coming from a stellar surface patch dS per second, and ρ_{GJ} is the Goldreich–Julian charge density (Goldreich & Julian 1969). We then binned $dL_\gamma/(E_{\text{CR}}dE)$ according to E_{CR} (see Equation (9)) for an energy bin size of dE , and divided by $dA = 2\pi d^2 \sin \zeta d\zeta$, with d the distance to the pulsar and ζ the observer’s line of sight measured with respect to the rotation axis, in order to obtain the phase-averaged photon spectrum with units $1/(\text{erg s cm}^2)$ (Venter 2008):

$$\frac{dN}{dE}(E, \chi, \zeta) = \frac{1}{dAdE} \iiint_{\zeta-d\zeta/2}^{\zeta+d\zeta/2} \left[\frac{dL_\gamma}{d\phi dE d\zeta} \right] \times \frac{I(E, dE)}{E_{\text{CR}}} d\phi dE d\zeta, \quad (20)$$

with χ the magnetic inclination angle. Integration takes place over all observer phases of radiation ϕ , some nar-

row strip in observer angle ζ , and all photon energies E ; $I(E, dE)$ is the indicator function which is nonzero only if $E_{CR} \in (E, E + dE)$.

One may view this technique as a method approximating single primary CR photon spectra by delta functions positioned at E_{CR} , and with integrated values (areas) $dL_\gamma/(E_{CR}dEdA)$. This approximation indeed saves time, as a single-particle CR spectrum (over many photon energies) is approximated by only one point (at one photon energy), and yields values that are reasonably close to more complicated and time-consuming calculations of CR gamma-ray integral fluxes and photon spectra. This is especially true for population studies, where the computation time may become very long when using several parameters and a fine parameter grid, as well as large numbers of population members. Also, the correct value of the total radiated CR gamma-ray power is preserved in the resulting gamma-ray spectra (and may be recovered as the first energy moment of the photon spectrum times dA). An example of spectral results obtained using this method may be seen in Figure 2 of Venter & de Jager (2005) as well as in Figure 2 of Venter & de Jager (2008).

4.2. Spectral Shape Fitting and Renormalization

It has however been pointed out (J. Dyks 2008, private communication) that the method described in the previous Section for calculating CR spectra using delta functions is somewhat crude. One loses the ‘‘spread’’ of the radiation over many photon energies when one ignores both the LE and HE tails of these single-particle spectra. This method therefore leads to very hard LE spectral tails, as well as very abrupt HE cutoffs. Both of these features imply that the resulting spectra do not compare very well to similar calculations (e.g., Frąckowiak & Rudak 2005; Harding et al. 2005). Addition of LE tails should lead to a cumulative E^2dN/dE -spectrum with an LE slope of 4/3 (Rudak & Dyks 1999) when ρ_c is slowly changing, while addition of HE tails should lead to a broader cumulative spectral cutoff.

To solve this problem, we proposed (Venter 2008) the following correction to transform the values of $E^2dN/dE(E_i) \equiv Y_i$ to Y'_i , a corrected CR spectrum (where $i = 0, 1, 2, \dots, N - 1$ signifies the i th energy bin and E_i the average energy associated with bin i). First, we approximate the νF_ν CR power spectrum using

$$E^2 \frac{dN}{dE} = \frac{E}{dA} \left(\frac{dP}{dE} \right)_{CR} \approx K E^{4/3} \exp\left(-\frac{E}{E_c}\right), \quad (21)$$

as motivated by the approximate forms of the $\kappa(x)$ function (see Equation (12), and also Equations (14) and (15); also note that Story et al. 2007 consider the LE approximation, without exponential cutoff, as suitable for their pulsar population study). We note that each point of the spectrum Y_i (dashed line in Figure 2) represents the addition of many single CR (delta) spectra, where only the total power has been used, as explained in Section 4.1. The full CR spectra should however have been used. It is reasonable to argue that the sum of full CR spectra at bin i may be approximated by one full (cumulative) CR spectrum with characteristic energy $E_c = E_i$ if the bin size dE is small enough, and with normalization as given by the sum of delta functions of the particular energy bin. In this case, all the spectra in the i th bin have very similar cutoff energies, and the result would be very close to the form of a single-particle spectrum. This leads to the following expression for

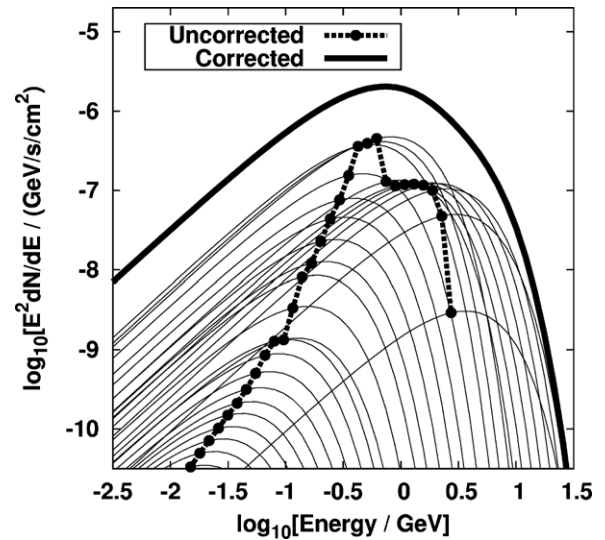


Figure 2. Correction of the cumulative CR spectrum Y_i resulting from summation of delta function approximations (thick dashed line). The thin lines are the approximate spectra $K_i E_i^{4/3} \exp(-E_j/E_i)$ fitted through each point (E_i, Y_i) . The thick solid line represents the corrected spectrum Y'_i (not normalized), which is the sum of all such spectra (thin lines).

each (relative) normalization constant K_i of the total spectrum for the i th bin, using Equation (21):

$$K_i = \frac{Y_i}{E_i^{4/3} \exp(-1)}. \quad (22)$$

To rectify our neglect of full CR spectra, we fit full spectra (thin solid lines in Figure 2) through each point (E_i, Y_i) , and then calculate the final CR spectrum Y'_i by adding all these cumulative CR spectra:

$$Y'_i = \sum_{j=0}^{N-1} K_j E_i^{4/3} \exp\left(-\frac{E_i}{E_j}\right). \quad (23)$$

Therefore, at each E_i , we take into account the contributions from all fitted spectra peaking near E_j to obtain the correct level of Y'_i . (For the special case when $j = i$, we recover Y_i using the definition of K_i , and add this to the series above.) This calculation leads to the thick solid line in Figure 2.

We finally normalize Y'_i using the total (correct) luminosity represented by the νF_ν -spectrum Y_i . We calculate (see the Appendix)

$$L_1 = \int_0^\infty E \left(\frac{dN}{dE} \right) dE \approx \sum_{i=0}^{N-1} \frac{Y_i}{E_i} \delta E_i = \delta \sum_{i=0}^{N-1} Y_i, \quad (24)$$

$$L_2 \approx \delta \sum_{i=0}^{N-1} Y'_i, \quad (25)$$

and finally multiply Y'_i by the factor L_1/L_2 . This gives the corrected, normalized CR spectrum indicated by the dashed line in panel (a) of Figure 3. Integration of the photon spectrum, using a variable lower energy limit E , gives the total flux above E :

$$F(> E) = \int_E^\infty \left(\frac{dN}{dE} \right) dE. \quad (26)$$

The various integral fluxes are indicated in panel (b) of Figure 3.

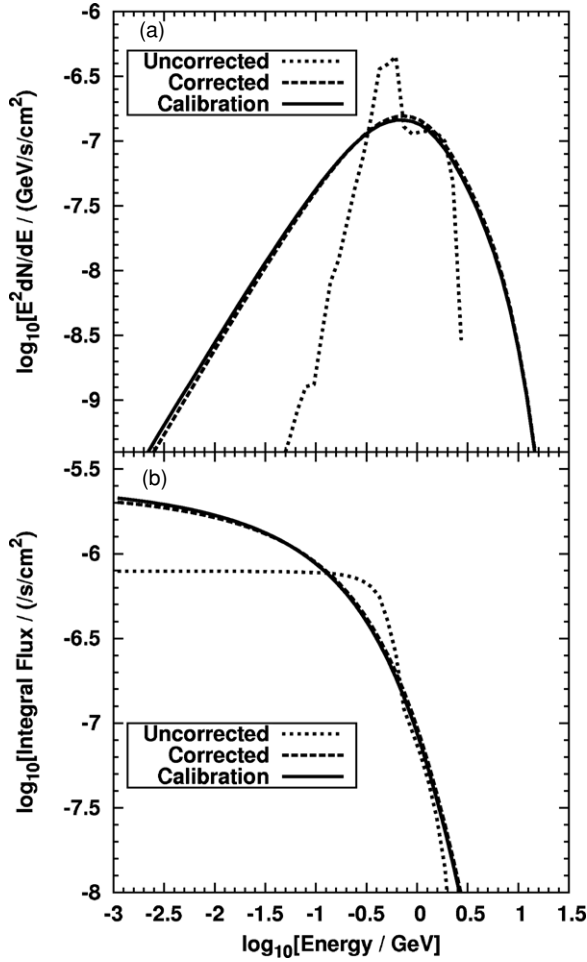


Figure 3. Comparison of uncorrected (Y_i ; short-dashed line), corrected ($Y_i L_1/L_2$; dashed line), and calibration (full calculation; solid line) CR spectra. Panel (a) indicates $E^2 dN/dE$, while (b) indicates the integral flux $F(>E)$. We used pulsar parameters typical of PSR J0437–4715 (stellar radius $R = 1.5 \times 10^6$ cm, pulsar mass $M = 1.58 M_\odot$, inclination angle $\alpha = 35^\circ$, and observer angle $\zeta = 40^\circ$; see Venter & de Jager 2005).

5. RESULTS: APPROXIMATION ACCURACY AND CODE SPEED INCREASE

We have compared the corrected spectra (dashed lines in Figure 3) with a full calculation of the cumulative CR spectrum (i.e., using $(dP/dE)_{\text{CR}}$ with no approximations; solid lines in Figure 3) and found that the resulting spectra are very similar. We used pulsar parameters typical of the MSP PSR J0437–4715 for illustrative purposes.

To get a quantitative measure of the goodness of fit, we used the mean integrated square error (MISE):

$$\text{MISE} \equiv \left\{ \frac{1}{b-a} \int_a^b \left[\frac{f(x) - \hat{f}(x)}{f(x)} \right]^2 dx \right\}^{1/2}, \quad (27)$$

with \hat{f} the approximation to f , and $a = E_{\min}$, $b = E_{\max}$. We calculated the MISE value using the $E^2 dN/dE$ spectra, and integrating up to three times the energy corresponding to the spectral maximum. The result is 0.070 (i.e., 7.0% relative error), indicating a very good fit, as can be inferred qualitatively from panel (a) of Figure 3.

The spectral calculation is only a part of a full pulsar radiation code, which calculates the radiated intensity as function of observer angle ζ and phase ϕ . In order to analyze the increase in speed for the total code when using the spectral approximation method (which is different from the increase in speed for the spectral part of the code only), let us write down the total time the full and approximate codes take:

$$t_{\text{full}} = t_A + t_{\text{CR,full}} \quad (28)$$

$$t_{\text{approx}} = t_A + t_{\text{CR,approx}} + t_{\text{correction}} \approx t_A + t_{\text{CR,approx}}, \quad (29)$$

with $t_{\text{CR,full}}$ and $t_{\text{CR,approx}}$ the time it takes to compute the CR spectrum in each case, and t_A the time it takes to do the rest of the calculations, e.g., calculating the B -field, E -field, and particle transport. The term $t_{\text{correction}}$ represents the time it takes to correct the cumulative delta spectrum Y_i by fitting spectra through each bin, as explained in Section 4.2; this is negligible compared to the other times (only a few seconds), and will be discarded in what follows. Next, define

$$\alpha \equiv \frac{t_{\text{approx}}}{t_{\text{full}}}, \quad \beta \equiv \frac{t_{\text{CR,approx}}}{t_{\text{CR,full}}}, \quad f \equiv \frac{t_{\text{CR,full}}}{t_{\text{full}}}. \quad (30)$$

The first two of these ratios are measurable, and may be used to find f (using $t_{\text{full}} - t_{\text{approx}}$):

$$f = \frac{1 - \alpha}{1 - \beta}. \quad (31)$$

The latter is the fraction of time t_{full} it takes to do the full spectral calculations. We obtained $\beta \approx (3.15 N_{\text{bins}})^{-1}$, which is a factor ~ 300 increase in the speed of the spectral calculation using $N_{\text{bins}} = 100$ bins, and a factor ~ 3000 increase for $N_{\text{bins}} = 1000$. This value of β leads to $\alpha \approx 0.33$, implying an overall increase in speed of a factor of 3. This gives $f \approx 0.67$, meaning that $t_A \equiv (1 - f)t_{\text{full}} \approx 0.33 t_{\text{full}}$. Once we have f , we can see that even if $1/\beta$ is very large (representing a significant increase in the speed of the spectral calculation by using an approximation method, as compared to a full CR calculation), there is a limit to the increase of the speed of the total code $1/\alpha$, since

$$\frac{1}{\alpha} = \frac{t_A + f t_{\text{full}}}{t_A + \beta f t_{\text{full}}} \approx 1 + \frac{f}{1 - f} = \frac{1}{1 - f}, \quad \beta \ll 1. \quad (32)$$

Therefore, the only way to increase the total gain in speed ($1/\alpha$) any further would be to increase f , i.e., to decrease the relative amount of time it takes to do the rest of the calculations. Thus, t_A limits any further increases in overall speed. There are at least two ways to decrease t_A , and therefore maximize the impact of the proposed spectral approximation technique. In the case of very complicated magnetospheric structure, where the B -field and/or E -field have to be calculated numerically (and where the light cylinder and polar cap have to be found numerically; see, e.g., Dyks & Harding 2004), it may be wise to pre-calculate these fields for a range of (P, \dot{P}, χ) , where P and \dot{P} are the pulsar period and its time derivative, and save these results. Any recalculation of these fields are then unnecessary when performing a population study, as they may simply be read in from memory as required. Second, it may be useful to pursue analytic approximations for these fields. Both approaches may substantially reduce t_A , especially when repetitive calculations may be avoided or speeded up.

6. INTERPRETATION OF THE ENERGY CORRESPONDING TO THE MAXIMUM OF THE SPECTRAL ENERGY DISTRIBUTION (SED)

We have commented that observers routinely fit a power law plus exponential cutoff to the HE pulsar spectra (Equation (3)), with the observationally inferred cutoff energy E_c roughly coinciding with the spectral maximum on a νF_ν plot. When using Equation (21), one can easily show that the SED maximum occurs at $E_{\gamma, \max} \approx (4/3)E_c$ (Harding et al. 2005). It is tempting to associate E_c with E_{CR} (or even $E_{\gamma, \max}$), and indeed this is a reasonable approximation for making rough estimates. We alluded to this being done when associating the radiation-reaction-limited prediction of CR cutoff energy with E_c , and finding values that correspond particularly well to the *Fermi*-LAT results (Section 1). However, since the parameter b which characterizes the strength of the exponential cutoff is not always unity, one sees that this association is not perfect, since the spectrum has a more complicated shape. It is believed that the phase-averaged and phase-resolved spectra are the superposition of various single-particle CR spectra coming from different regions in the magnetosphere. Each single-particle CR spectrum depends on γ and ρ_c , both of which are a function of position (since E_{\parallel} and ρ_c determines γ , and the magnetic field structure determines ρ_c). In addition, relativistic aberration and time of flight delays play a role in determining the phase of the eventual radiated spectrum (Dyks & Rudak 2003). The different spectra therefore all have different respective intensities and cutoffs, and all of these add up to give a cumulative spectrum with spectral index softer than $-2/3$, and a broad exponential decay (and possibly a roll-over near E_c). Other components different from the CR component may also contribute to soften the observed spectral index. In view of this, it is important to remember that while there may be a relation between E_c and the cutoff energy of the most dominant single-particle CR spectra (i.e., those with highest E_{CR} and largest intensity), a unique association would be a simplification of a more realistic scenario where the observed CR spectrum represents a superposition of single-particle spectra reaching the observer from several different altitudes in the magnetosphere.

7. APPLYING THE APPROXIMATION METHOD TO SR

As mentioned in Section 1, one would expect that CR is not the only radiation mechanism operating in a typical pulsar magnetosphere. For example, pair creation of curvature photons leads to a cascade of electron-positron pairs which may radiate SR. The critical synchrotron frequency is given by

$$\omega_{\text{SR}} = \frac{3eB_{\perp}\gamma^2}{2m_e c}, \quad (33)$$

with $B_{\perp} = B \sin \alpha'$, and α' the pitch angle. Similar to Equation (10), we have the single-particle power spectrum (Rybicki & Lightman 1979)

$$\left(\frac{dP}{dE}\right)_{\text{SR}} = \frac{\sqrt{3}e^3 B_{\perp}}{hm_e c^2} \kappa \left(\frac{E_{\gamma}}{\hbar\omega_{\text{SR}}}\right), \quad (34)$$

with the spectral maximum occurring at $0.29\omega_{\text{SR}}$ (Longair 1994). The integral of Equation (34) yields the total SR energy loss rate (Blumenthal & Gould 1970):

$$\dot{E}_{\text{SR}} = -\frac{2(r_0\gamma B_{\perp}v_e)^2}{3c}, \quad (35)$$

with $r_0 = e^2/m_e c^2$ the electron radius, and v_e the electron speed. Due to the fact that $\kappa(x)$ is used in Equation (34) in much the same way as in Equation (10), we have the same approximate forms of Erber (1966) for $\kappa(x)$, so that the SR spectrum is also described by a power law at low energies, and an exponential cutoff for $\omega \gtrsim \omega_{\text{SR}}$. We therefore argue that, since the typical cutoff energy and total power of a single-particle spectrum are known for SR, just as in the case of CR, and the modified Bessel function is used in both cases to compute the spectra, the approximation method described in Section 4.2 may be also applied to SR: one may use delta functions of total power situated at the critical frequency as “placeholders,” and later correct for the full SR spectrum, either using Equation (21), the approximations of Equation (12), or tabulated values of $\kappa(x)$.

The general case of inverse Compton scattering (ICS) in an anisotropic radiation field is quite complicated (Blumenthal & Gould 1970), and implementing an approximation technique similar to what we have done for CR and SR is outside the scope of this paper.

8. CONCLUSION

We have argued that CR and SR radiation are essential and ubiquitous in all pulsar models (and even for other astrophysical sources where these mechanisms, especially the latter, are invoked; also in a multiwavelength context) and that the observed (cumulative) spectra are believed to be the result of many millions of single-particle spectra. Even in the case of, e.g., synchrotron self-Compton radiation, one may view the respective processes of ICS and SR as independent, as long as the soft radiation fields, the scattering of the soft photons to HE photons, pair production and SR, with associated particle energy losses, are self-consistently calculated. In view of several potential applications where significant spectral computation is needed, it is therefore useful to find an approximation technique which preserves accuracy when predicting cumulative CR and SR spectra.

We summarized the standard CR expressions, noting typographical errors in the literature, and also calibrated the spectral part of our code by reproducing the LE and HE CR spectral approximations. Next, we found that we could increase the speed of our radiation code (for calculating spectra for all observers) by a factor of ~ 3 , while the results are very close to calculations using the standard expressions. There are several applications where this increase in speed will be useful. Some examples include calculation of so-called phase plots (plots of intensity versus observer angle ζ and phase ϕ ; see, e.g., Romani & Yadigaroglu 1995), from which light curves are created by making constant- ζ slices; performing a parameter study for a population of pulsars, which will require spectra and light curves for several observers; and calculation of the geometric factor f_{Ω} used for converting observed energy flux to total gamma-ray luminosity (Watters et al. 2009).

If only the observed flux for one specific observer at fixed ζ is required, and not the flux or luminosity for the whole sky (i.e., all ζ), we found that the spectral calculation is only done for $\sim 2\%$ of the time. In this case, the major increase in speed for the spectral part of the code (a factor of $\sim 3N_{\text{bins}}$) is not reflected in the time the total code takes, as the total time drops by at most 2% (i.e., the spectral calculation time is negligible), leading to a negligible increase in speed of a factor of $1/0.98 \approx 1.02$. The approximation method is therefore not as suitable for observer-specific applications.

Our approximation scheme will work over the full range of energies and will not lose any accuracy by only invoking an LE or HE approximation of the $\kappa(x)$ function when calculating the SR or CR spectra (e.g., Harding et al. 2005; Story et al. 2007; Harding et al. 2008). Furthermore, using a spectral shape very close to that implied by the standard expressions when correcting our cumulative spectra as described above leads to broader HE tails of the CR spectra as compared to using the delta-approximation. This is an important improvement of our HE CR flux predictions, as future ground-based telescopes such as the next-generation High Energy Stereoscopic System and Cherenkov Telescope Array may possibly probe the tails of CR spectra from pulsar candidates (J. Dyks 2008, private communication). We have therefore adopted this correction for future work, e.g., to explain cumulative CR radiation from MSPs in globular clusters (Venter et al. 2009a). Lastly, a full ICS calculation will have to be done after the CR and SR spectra have been corrected, until a similar approximation technique has been developed for the ICS process.

This work is based on research supported by the South African Research Chairs Initiative of the Department of Science and Technology and National Research Foundation. We thank the Aspen Center for Physics for providing the opportunity to complete this manuscript.

APPENDIX

LOGARITHMIC INTEGRATION

We outline a formula for numeric integration of a function $f(E)$ using logarithmically spaced E -values, and referred to as “logarithmic integration” in the text:

$$\int_{E_{\min}}^{E_{\max}} f(E) dE \approx \sum_{k=0}^{N-1} f_k \Delta E_k. \quad (\text{A1})$$

First, we specify a logarithmically spaced energy vector:

$$E_k = E_0 e^{k\delta}, \quad k = 0, 1, \dots, N-1, \quad (\text{A2})$$

with $E_0 \equiv E_{\min}$ and $E_{N-1} \equiv E_{\max}$. It then follows that

$$\delta = \frac{\ln(E_{\max}/E_{\min})}{N-1}. \quad (\text{A3})$$

One may also construct an average energy

$$E_{\text{avg},k} = \frac{1}{2}(E_k + E_{k-1}) = \frac{1}{2}E_0(e^{k\delta} + e^{(k-1)\delta}) \quad (\text{A4})$$

for the energy bin spanning $[E_{k-1}, E_k]$, $k = 1, 2, \dots, N-1$, with width

$$dE_k = E_k - E_{k-1} = E_0(e^{k\delta} - e^{(k-1)\delta}). \quad (\text{A5})$$

Assuming k to be a continuous variable for the moment,

$$\frac{dE_k}{dk} = \delta E_k. \quad (\text{A6})$$

Setting $dk = 1$, we find

$$dE_k \approx \delta E_k. \quad (\text{A7})$$

This result can also be derived when k is a discrete value (and δ is small):

$$\Delta E = (E_k - E_{k-1}) \quad (\text{A8})$$

$$= E_0 e^{k\delta} (1 - e^{-\delta}) \quad (\text{A9})$$

$$= E_0 e^{k\delta} (1 - (1 - \delta - \dots)) \quad (\text{A10})$$

$$\approx \delta E_k. \quad (\text{A11})$$

We can now obtain an approximate integration formula:

$$\int_{E_{\min}}^{E_{\max}} f(E) dE \approx \sum_{k=0}^{N-1} f_k \delta E_k = \delta \sum_{k=0}^{N-1} f_k E_k, \quad (\text{A12})$$

with $f_k = f(E_k)$ or $f_k = f(E_{\text{avg}}, k)$.

REFERENCES

- Abdo, A. A., et al. 2009, *Science*, **325**, 845
 Abdo, A. A., et al. 2010a, *ApJS*, **187**, 460
 Abdo, A. A., et al. 2010b, *ApJ*, **713**, 154
 Abdo, A. A., et al. 2010c, arXiv:1003.3588
 Arons, J. 1983, *ApJ*, **266**, 215
 Blumenthal, G. R., & Gould, R. J. 1970, *Rev. Mod. Phys.*, **42**, 237
 Bulik, T., Rudak, B., & Dyks, J. 2000, *MNRAS*, **317**, 97
 Cheng, K. S., Ho, C., & Ruderman, M. 1986, *ApJ*, **300**, 500
 Cheng, K. S., & Zhang, J. L. 1996, *ApJ*, **463**, 271
 Daugherty, J. K., & Harding, A. K. 1982, *ApJ*, **252**, 337
 Daugherty, J. K., & Harding, A. K. 1996, *ApJ*, **458**, 278
 Dyks, J., & Harding, A. K. 2004, *ApJ*, **614**, 869
 Dyks, J., & Rudak, B. 2003, *ApJ*, **598**, 1201
 Erber, T. 1966, *Rev. Mod. Phys.*, **38**, 626
 Frackowiak, M., & Rudak, B. 2005, *Adv. Space Res.*, **35**, 1152
 Goldreich, P., & Julian, W. H. 1969, *ApJ*, **157**, 869
 Harding, A. K. 1981, *ApJ*, **245**, 267
 Harding, A. K., Stern, J. V., Dyks, J., & Frackowiak, M. 2008, *ApJ*, **680**, 1378
 Harding, A. K., Usov, V. V., & Muslimov, A. G. 2005, *ApJ*, **622**, 531
 Hirotani, K. 2005, *Adv. Space Res.*, **35**, 1085
 Jackson, J. D. 1962, *Classical Electrodynamics* (New York: Wiley)
 Longair, M. S. 1994, *High-Energy Astrophysics*, Vol. 2 (2nd ed.; Cambridge Univ. Press)
 Mészáros, P. 1992, *High-Energy Radiation from Magnetized Neutron Stars* (Chicago, IL: Univ. Chicago Press)
 Muslimov, A. G., & Harding, A. K. 2003, *ApJ*, **588**, 430
 Nel, H. I., & De Jager, O. C. 1995, *Ap&SS*, **230**, 299
 Romani, R. W. 1996, *ApJ*, **470**, 469
 Romani, R. W., & Yadigaroglu, I.-A. 1995, *ApJ*, **438**, 314
 Rudak, B., & Dyks, J. 1999, *MNRAS*, **303**, 477
 Rybicki, G. B., & Lightman, A. P. 1979, *Radiative Processes in Astrophysics* (New York: Wiley)
 Story, S. A., Gonthier, P. L., & Harding, A. K. 2007, *ApJ*, **671**, 713
 Venter, C. 2008, PhD thesis, North-West Univ., Potchefstroom Campus
 Venter, C., & de Jager, O. C. 2005, *ApJ*, **619**, L167
 Venter, C., & de Jager, O. C. 2008, *ApJ*, **680**, L125
 Venter, C., De Jager, O. C., & Clapson, A.-C. 2009a, *ApJ*, **696**, L52
 Venter, C., Harding, A. K., & Guillemot, L. 2009b, *ApJ*, **707**, 800
 Watters, K. P., Romani, R. W., Weltevrede, P., & Johnston, S. 2009, *ApJ*, **695**, 1289